Journal of Materials Chemistry A

Accepted Manuscript

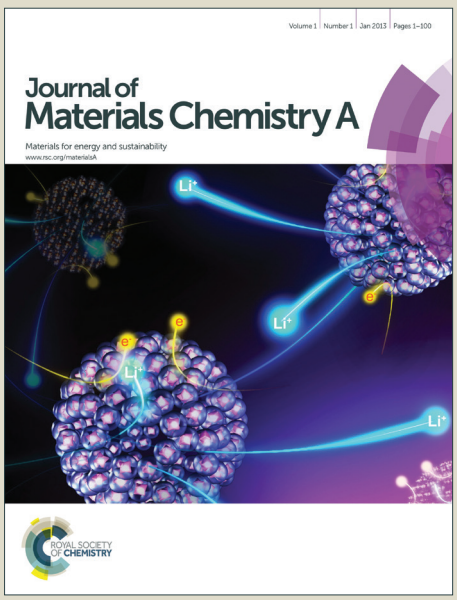

ROYAL SOCIETY OF CHEMISTRY

www.rsc.org/materialsA

Hierarchical $NiCo_2O_4$ nanosheets decorated carbon nanotubes towards highly efficient electrocatalyst for water oxidation

Hui Cheng, Yu-Zhi Su, Pan-Yong Kuang, Gao-Feng Chen, Zhao-Qing Liu*

Received (in XXX, XXX) Xth XXXXXXXXX 20XX, Accepted Xth XXXXXXXXX 20XX
DOI: 10.1039/b000000x

The development of robust and low cost electrocatalysts with highly efficient oxygen evolution reaction capability remains a great challenge for widespread applications toward the water splitting. Here, the spinel $NiCo_2O_4$ nanosheets grown on the mildly oxidized multi-walled carbon nanotubes (CNTs) have been synthesized via a simple one-pot solution method. Compared with the pure $NiCo_2O_4$, the as-prepared hierarchical $NiCo_2O_4$/CNTs composite exhibits superior OER catalytic properties, *i.e.* more negative onset potential, smaller Tafel slope and higher stability, which may be attributed to the enhanced conductivity of the hybrid originating from the carbon nanotubes substrate. Furthermore, the surface Co/Ni ratio of $NiCo_2O_4$/CNTs is rebuilt by the synergistic reactivity between oxygen-enriched groups and metal ions, which thereby improves the catalytic performance of $NiCo_2O_4$/CNTs. Such electrocatalyst with enhanced electrocatalytic performances for OER may be a promising candidate for the water splitting.

Introduction

With the ever-increasing depletion of fossil fuels and the continuing deterioration of environmental pollutions, the development of alternative energy conversion or storage devices with high power and large energy densities is of particular significance.[1,2] Among them, oxygen evolution reaction (OER) enables many energy storage options such as electricity-driven and/or direct-solar water splitting as an important process, but it is sluggish in the kinetics even after being facilitated by noble-metal catalysts. In addition, the anodic reaction of OER process is complex, in which the hydroxyl ions are consumed to produce oxygen and water molecules ($4OH^- \leftrightarrow O_2 + 2H_2O + 4e^-$) requiring a considerable overpotential in alkaline condition.[3,4] However, the practical implementation of water splitting is severely constrained by the efficiency-limited OER.[5-7] Thus, an important issue for OER is the development of catalysts that can reduce the overpotential.

Heretofore, noble-metal based catalysts such as IrO_2 and RuO_2 are the most active catalysts, but their widespread applications in real industry are hindered owing to their scarcity and high cost.[8] Therefore, extensive research efforts have been devoted to seeking inexpensive and efficient OER electrocatalysts with superior OER performances and sufficient stability. To date, it has been reported that spinel cobalt-based oxides are the most promising electrocatalysts in alkaline electrolyte, due to the prominent advantages of low price, easy preparation, high activity, excellent stability as well as environmental friendliness.[9-11] Furthermore, the electrocatalytic efficiency of Co_3O_4 could be improved by doping with metal ions, such as Fe, Zn, Cu, Ni.[12-15] Among these, the spinel binary nickel cobaltite, having various applications in the fields of lithium ion batteries,[16,17] fuel cells,[18,19] magnetic materials[20,21] and electrochemical capacitors,[22] *etc.*, has aroused much attention and has been employed as the water oxidation catalyst because of its outstanding electrocatalytic activity and stability in alkaline condition.[23,24] The Ni doping enables $NiCo_2O_4$ to possess a much better electronic conductivity (at least 2 orders of magnitude higher than that of Co_3O_4) and more active sites for OER.[25-26] More importantly, due to the different valence state in the spinel structure where Ni occupies the octahedral sites and Co occupies both the octahedral and the tetrahedral sites, both the redox couples (*i.e.* Co^{3+}/Co^{2+} and Ni^{3+}/Ni^{2+}) ensure a notable electrocatalytic activity. Despite the improved catalytic activity of $NiCo_2O_4$, it is highly desirable to further enhance its catalytic performances for practical applications. In virtue of their reinforced synergistic effects, one of effective strategies is depositing $NiCo_2O_4$ on conductive supports with excellent conductivity and high surface area.[27]

Carbon nanotubes (CNTs), as an important class of nanocarbon materials, have excellent conductivity, high specific surface area, chemical stability, very high strength and low density, making them as useful substrates to produce hybrid and composite materials for various applications. In particular, many multi-walled CNTs based composites have been explored as advanced electrocatalysts.[28-30] As for OER application, a variety of transition metal compounds, such as non-precious metal,[31] MnO_2,[32] and $MnCo_2O_4$,[33] have been grown on CNTs in attempt to boost the OER catalysis, which have been demonstrated as a feasible and effective approach. Therefore, constructing $NiCo_2O_4$/CNTs composite with hierarchical structure could be an attractive potential OER electrocatalyst. Furthermore, to the best of our knowledge, there is still no report on the synergistic catalytic mechanism of $NiCo_2O_4$ /CNTs in the OER process.

Herein, we report the spinel $NiCo_2O_4$ on the oxidized multi-walled CNTs as an active electrocatalyst for OER by a facile solution method. The introduced multi-walled CNTs could provide huge surface area for the growth of $NiCo_2O_4$ nanosheets and contribute to the outstanding conductivity. Benefiting from these features, the hierarchical $NiCo_2O_4$/CNTs exhibits superior OER catalysis compared with the pure $NiCo_2O_4$ and $NiCo_2O_4$/activated carbon (AC) composite. To gain insight into the growth mechanism of $NiCo_2O_4$ on CNTs, both the multi-

walled CNTs with oxidization and without oxidization are adopted as substrates. The comparison result indicates that the oxidization pre-treatment CNTs with oxygen-enriched groups like —OH and —COOH play an essential role in modifying the surface of $NiCo_2O_4$, leading to the increased ratio of Co/Ni in $NiCo_2O_4$/CNTs as well as further enhanced OER activity. The superior performance is credited to the unique micro-structure and the prominent synergistic effects of the components. In view of the highly improved catalytic efficiency in OER, $NiCo_2O_4$/CNTs composite demonstrates a very promising candidature as electrocatalyst for the water splitting.

Experimental

Chemicals and materials

All reagents used in the experiment were of analytical grade and were used without further purification. $Ni(NO_3)_2 \cdot 6H_2O$ (99% AR), $Co(NO_3)_2 \cdot 6H_2O$ (99% AR) and active carbon were obtained from Guangzhou Chemical Reagent Factory and Tianjin Fuchen Chemical Reagent Factory, respectively. Polyvinylpyrrolidone (PVP, 99% AR) and $NH_3 \cdot H_2O$ (25-28 wt %) were obtained from Shanghai Tianlian Fine Chemical Co. Ltd. and Tianjin Fuyu Fine Chemical Co. Ltd., respectively. The multi-walled carbon nanotubes (CNTs, 99% AR) were purchased from Shenzhen Nanotech Port Co. Ltd..

Oxidization of multi-walled carbon nanotubes

1 g of the multi-walled CNTs was purified by washing with 70 mL of the diluted hydrochloric acid (10 wt %) to remove metal residues. The products were then filtered, washed and dried. After that, 23 mL of the concentrated sulfuric acid was added to the purified multi-walled CNTs in a 250 mL round-bottom flask, and the mixture was stirred at the room temperature overnight. Next, the solution was transferred to an oil bath. After its temperature was raised to 40 °C, 416 mg of KNO_3 was added, followed by the slow addition of 1 g of $KMnO_4$ while keeping the reaction temperature below 45 °C. The solution was kept stirring at 40 °C for 30 min. Subsequently, 3 mL of water was added to the flask, followed by another 3 mL of water after 5 minutes. After another 5 minutes, 40 mL of water was added. 15 minutes later, the flask was removed from the oil bath and 140 mL of water and 10 mL of 30% H_2O_2 were added to terminate the oxidization reaction. The oxidized multi-walled CNTs were collected, repetitively washed with 5 % HCl solution and water, and finally lyophilized. The yield for the oxidized carbon nanotubes was 86.5%.

Synthesis of $NiCo_2O_4$ nanosheets on the oxidized multi-walled carbon nanotubes

In a typical solution process, 0.58 g of $Ni(NO_3)_2 \cdot 6H_2O$ and 1.16 g of $Co(NO_3)_2 \cdot 6H_2O$ were dissolved into 50 mL H_2O to form a clean purple solution, which was mixed with 0.35 g PVP. After that, 0.21 g of the oxidized multi-walled CNTs powder was uniformly dispersed in the aqueous solution under the assistance of the ultrasonication at 400 W for 0.5 h. Then, $NH_3 \cdot H_2O$ (5 %) was added dropwise until its pH reached 9. The obtained precipitate was filtered, washed with water and ethanol several times to remove the surfactant and residual ions, and dried at 70 °C for 12 h under vacuum. Finally, the hybrid precursor was annealed in air at 200 °C for 3 h with a slow heating rate of 1 °C min^{-1}. The yield for the catalyst is 95%. The obtained catalyst ($NiCo_2O_4$: 70 wt %) is denoted as $NiCo_2O_4$/CNTs. Meanwhile, The hybrids with $NiCo_2O_4$ contents of 90, 80, 60, 50 wt % were prepared by the similar method. For comparison, $NiCo_2O_4$ (70 wt %) grown on activated carbon (denoted as $NiCo_2O_4$/AC) was synthesized by the similar synthesis procedures except that the oxidized multi-walled CNTs were substituted by AC. $NiCo_2O_4$ (70 wt %) grown on the pristine multi-walled CNTs (denoted as $NiCo_2O_4$/pCNTs) was synthesized through the similar method except the multi-walled CNTs with no pre-treatment. The bare $NiCo_2O_4$ was prepared by the similar synthesis procedures without the addition of the oxidized multi-walled CNTs. In addition, the physical mixture of $NiCo_2O_4$ and CNTs was also prepared. The calcined spinel $NiCo_2O_4$ (0.21 g) was physically mixed with 30 wt % CNTs (0.09 g). The mixture was heated under a nitrogen flow at 200 °C for 1h and allowed to cool naturally to room temperature.

Characterizations

The surface morphology and structure of the as-prepared samples were analyzed by using field emission scanning electron microscopy (FE-SEM, Quanta 400) and transmission electron microscopy (TEM, 300 kV, Tecnai™ G2 F30). The structure of the samples were analyzed by powder X-ray diffraction (XRD, Bruker , D8 ADVANCE) with Kα radiation (λ = 1.5418 Å). The chemical-state analysis of samples was carried out by X-ray Photoelectron Spectroscopy (XPS, ESCALab250). The specific surface area and the pore size distribution of the sample were investigated by the Brunauer-Emmett-Teller (BET). Thermogravimetric analysis (TGA, SDT 2960,) was used to estimate the mass content of the carbon in $NiCo_2O_4$/CNTs.

Electrochemical measurements

The electrochemical properties of the as-prepared samples were investigated by employing a CHI 760D electrochemical workstation (Chenhua, Shanghai) in a three-compartment cell with a Pt plate counter electrode, a saturated calomel electrode (SCE) reference electrode, and a working electrode. The electrolyte was 1 M aqueous solution of KOH. The working electrode was prepared as follow: 20 mg of the catalyst were dispersed in 100 mL of DI water, and 45 mL of PTFE was added. The contents were dispersed, followed by ultrasonication for approximately 30 min to obtain a homogeneous suspension. 0.48 mL of the catalyst ink was dropped on the surface of the glassy carbon disk (working electrode) and dried at room temperature, leading to a catalyst loading of 0.2 mg cm^{-2}. Polarization curves were recorded with the scan rate of 1 mV s^{-1}. The working electrodes were scanned for several times until the signals were stabilized, and then the data were collected. Cyclic voltammetry was conducted with the scan rate of 5 mV s^{-1} in the range of 0 to 0.5 V. Electrochemical impedance spectroscopy (EIS) was carried out in the frequency range of 0.01 Hz to 0.10 MHz at 0.56 V. The stability was characterized by the chronoamperometry which was carried out at 0.56 V. Tafel slopes were derived from polarization curves. The Tafel slope was calculated according to Tafel equation as follows: $\eta = a + b \cdot \log j$, where η denotes the overpotential, a denotes as Tafel constant, b denotes the Tafel slope, j denotes the current density. The overpotential was calculated as follows: $\eta = E$ (*vs.* SCE) –

0.16, considering O_2 / OH^- equilibrium in 1M KOH solution at 0.16 V *vs.* SCE.

Calculation of overpotential η

$E^0 = 1.230\ V - (0.059V)\ pH$, pH of 1 M KOH = 14

$E^0 = 1.230\ V - (0.059V) \times 14 = 0.404\ V$ *vs.* RHE

SCE (saturated KCl) *vs.* RHE = 0.244 V

$E^0 = 0.404 - 0.244 = 0.16\ V$ *vs.* SCE

Overpotential $\eta = E$ (*vs.* SCE) – 0.16 V

Result and discussion

The mechanism of the $NiCo_2O_4$ growth is shown in Scheme 1. It is well known that the external carbon-net of multi-walled CNTs have some of breaches, on which the oxygen-enriched groups such as hydroxyl and carbonyl exist (State Ⅰ). Accompanying the oxidization, more gaps are breached and the amount of these kinds functional groups increase.[34] Amongst of these oxygen-enriched groups, carboxyl group, the main functional group in the oxidized multi-walled CNTs, has the ability to coordinate the Ni^{2+} cation and the Co^{2+} cation (State Ⅱ). With the addition of the ammonium hydroxide drop by drop, the metal cations near the carboxyl group generate precipitations prior (State Ⅲ).[31] After the functional groups are covered, the remainder metal caions finally generate the precipitation to wrap the former (State Ⅳ).

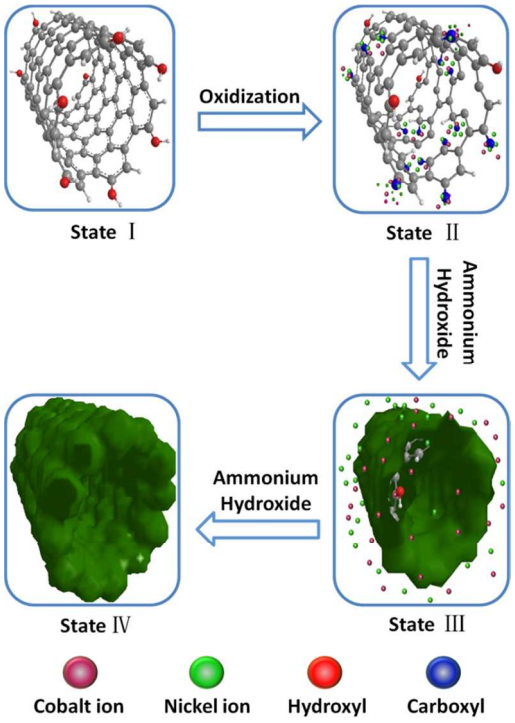

Scheme 1. Scheme illustrating the hydroxide growth of hierarchical $NiCo_2O_4$/CNTs composite.

The XRD measurement was used to identify the chemical composition and the phase of $NiCo_2O_4$/CNTs. As presented in Figure 1, the obtained diffraction peaks match well with the standard patterns of the spinel $NiCo_2O_4$ phase (JCPDS card No. 20-0781) and no other peaks are observed, which effectively confirms that the one-dimensional multi-walled CNTs were completely wrapped by $NiCo_2O_4$. However, when the $NiCo_2O_4$ content decreases to certain value, the XRD features of CNTs can be observed (Figure S1).

The morphology of hierarchical $NiCo_2O_4$/CNTs was observed by SEM and TEM shown in Figure 2. As shown in Figure 2a and 2b, numerous nanosheets grow well around the individual multi-walled CNTs to form a flower-like coating on the surface. Meanwhile, the mutual contacts indicate that the nanosheets grew not only on the individual CNTs but also in the contact sites between CNTs, forming a better conductive network. Such hierarchical nanostructure, maintaining a conductive core, may be remarkably beneficial to the improvement of the specific surface area, which is of great importance to the electrochemical performance of electrode materials. Moreover, the interior structure of hierarchical $NiCo_2O_4$/CNTs was further investigated by TEM (Figure 2c-e). It can be clearly observed that the ultrathin nanosheets with large lateral size (around 100 nm width) growing around the multi-walled CNTs core. Such characteristics confirm the intimate contact between the nanosheets and the multi-walled CNTs scaffold. The corresponding HRTEM image of hierarchical $NiCo_2O_4$/CNTs in Figure 2f exhibits the lattice fringes with an interlayer distance of 0.29 nm, which corresponds to the (220) plane of $NiCo_2O_4$. The EDX elemental mapping analysis in Figure 3 clearly presents the composition and uniform distribution of cobalt, nickel of $NiCo_2O_4$/CNTs nanostructure throughout the hierarchical nanosheets, implying that the nanosheet is the typical spinel $NiCo_2O_4$ but not the simple mixing of cobalt oxide and nickel oxide. And it also reveals that the multi-walled CNTs were completely wrapped by the $NiCo_2O_4$. For comparison, the morphology of pure $NiCo_2O_4$ is also presented in Figure S2. As shown, the pure $NiCo_2O_4$ is comprised of nanosheets as well. However, it is clearly seen that the nanosheets agglomerate with each other without the multi-walled CNTs acting as a bone for $NiCo_2O_4$ nanosheets, resulting in a low specific surface area. This conclusion may be further confirmed by the specific surface area measurement. As revealed by the nitrogen adsorption-desorption measurement, the hierarchical $NiCo_2O_4$/CNTs has a high BET specific surface area of about 170 $m^2\ g^{-1}$ with a broad pore-size distribution and a large pore volume of 0.7 $cm^3\ g^{-1}$ (Figure 4a). And the pure $NiCo_2O_4$ has a relatively low BET specific surface area of about 105 $m^2\ g^{-1}$ and small pore volume of 0.4 $cm^3\ g^{-1}$ (Figure S3). This result provides additional

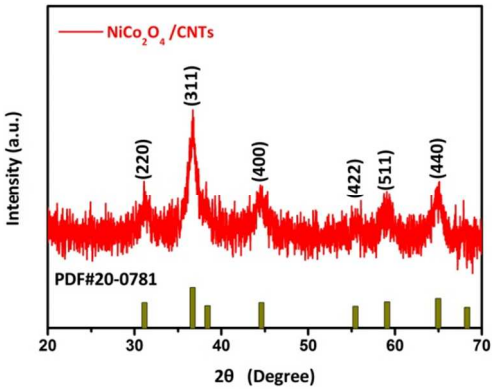

Figure 1. XRD pattern of the hierarchical $NiCo_2O_4$/CNTs.

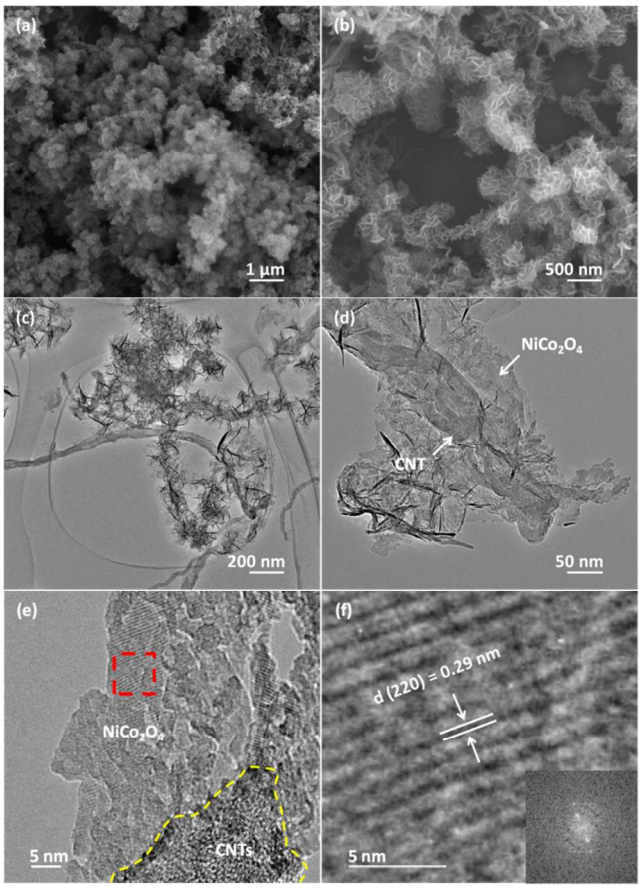

Figure 2. (a-b) SEM images, (c-d) TEM images and (e-f) HRTEM images of the hierarchical $NiCo_2O_4$/CNTs. The image (f) is taken from the region marked with the rectangle in panel (e).

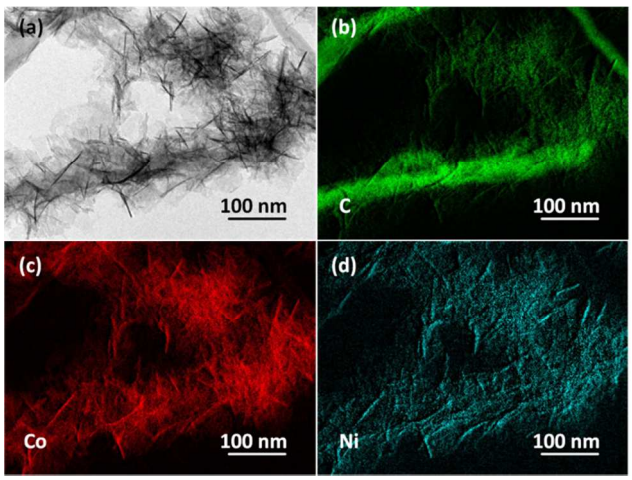

Figure 3. (a) HAADF-STEM image of hierarchical $NiCo_2O_4$/CNTs shows the structure morphology; (c-d) the corresponding energy-dispersive X-ray spectroscopy mapping.

proof that the higher specific area is induced by the multi-walled CNTs.

TGA/DTG measurements were used to evaluate the functional relationship between the mass change and the temperature (Figure 4b). As can be seen, only a slight weight loss before 200 °C, implying that CNTs including the oxygen-enriched groups could be retained during the annealing process at 200 °C for 3 h in air. The weight loss of about 12 wt % occurs from 210 °C to 245 °C, and the DTG peak at about 225 °C. This result can be attributed to the oxidization of the carboxyl group. In addition, the weight loss of about 15 wt % in the temperature range between 245 °C and 468 °C arises in the TG curve with a peak existing at about 400 °C in the DTG curve, which should be the reaction between CNTs and O_2.[35]

The electrochemical performances of hierarchical $NiCo_2O_4$/CNTs were investigated in Figure 5. Figure 5a shows the CV curves comparison of the hierarchical $NiCo_2O_4$/CNTs, $NiCo_2O_4$/AC, the physical mixture of $NiCo_2O_4$ and CNTs ($NiCo_2O_4$ + CNTs) and pure $NiCo_2O_4$. Obviously, the hierarchical $NiCo_2O_4$/CNTs have the similar feature of the redox peaks and OER onset potential with $NiCo_2O_4$/AC, while the curve of the pure $NiCo_2O_4$ is quite different. The negatively shift of the redox peaks and the onset potential may be attributed to the enhancement of conductivity by the carbon substrate. In addition, the CV curve of $NiCo_2O_4$/CNTs has additional redox peaks at 0.2 V compared to $NiCo_2O_4$/AC, which will be explained below. Notably, the curve of $NiCo_2O_4$ + CNTs possesses the similar feature compared to that of pure $NiCo_2O_4$, implying the weak synergetic effect between $NiCo_2O_4$ and CNTs in the physical mixture catalyst. Besides, the order of area sizes covered by the CV curve are listed as followed: $NiCo_2O_4$/CNTs > $NiCo_2O_4$/AC > $NiCo_2O_4$ + CNTs > pure $NiCo_2O_4$. It can be accounted for two reasons: (1) the carbon-substrate hybrid, with the enhancement of electrical conductivity induced by the carbon substrate, has a higher capacitance than pure $NiCo_2O_4$; (2) the diversity of carbon material, the multi-walled CNTs with carbon-net structure accelerates the charge transfer, but AC agglomerates bound together.

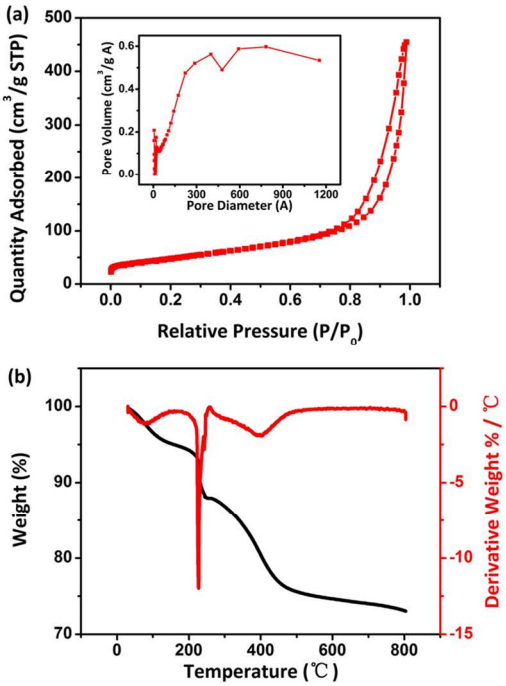

Figure 4. (a) Nitrogen adsorption-desorption isotherm of the hierarchical $NiCo_2O_4$/CNTs. The inset shows the pore-size distribution from the corresponding adsorption branch; (b) TGA/DTG measurement of the hierarchical $NiCo_2O_4$/CNTs in air with a temperature rate of 10 K min^{-1}.

The polarizations curves were further employed to evaluate the OER kinetics of the catalysts. Figure S4 shows that the OER activities are optimized for the hybrid catalyst consisting of 70 wt % $NiCo_2O_4$ and 30 wt % CNTs. Notably, even after the content of $NiCo_2O_4$ drop to 50 wt %, the hybrid maintains excellent performance compared to the pure $NiCo_2O_4$. As shown in Figure 5b, $NiCo_2O_4$/CNTs has the similar onset (about 0.5 V) with $NiCo_2O_4$/AC. However, it has a higher current density about 83 mA cm^{-2} at 0.7 V, three times higher than that of $NiCo_2O_4$/AC which declines dramatically at high potential. This result can be ascribed to the diversity of carbon materials that the carbon-net of the multi-walled CNTs mutual contact accelerates the charge transfer. In comparison, the accumulation of activated carbon existing separately induces the interrupt of the charge transfer. Besides, The $NiCo_2O_4$ on AC grew into pieces easily so that $NiCo_2O_4$/AC contains less number of effective or accessible OER active sites. In Figure 5b, the pure $NiCo_2O_4$ and the multi-walled CNTs show the OER activity as well, but neither the onset potential nor the current density is comparable to $NiCo_2O_4$/CNTs. And the physical mixture catalyst possesses poor OER activity, even worse than that of pure $NiCo_2O_4$. This result further confirms the weak synergetic effect in the catalyst. Thus, only $NiCo_2O_4$ plays a role in the OER catalytic effect in such the physically mixed catalyst. And with the decrease of the $NiCo_2O_4$ content, the OER activity declines simultaneously. The OER kinetics of the above catalysts are estimated by corresponding Tafel plots (log j-η) that the Tafel slope of $NiCo_2O_4$/CNTs is about 68.1 mV dec^{-1}, while 70 mV dec^{-1} for $NiCo_2O_4$/AC, 79.0 mV dec^{-1} for $NiCo_2O_4$ + CNTs, and 77.3 mV dec^{-1} for the pure $NiCo_2O_4$ (Figure 5c and Table S1). It demonstrates $NiCo_2O_4$/CNTs possesses an efficient kinetic for water oxidation. Since the OER activity of $NiCo_2O_4$/CNTs exhibits more negative onset potential, higher current and lower Tafel slope, the integration of $NiCo_2O_4$ with CNTs is an indication for the superior OER catalyst.

Ionic and charge transport is also an essential factor for efficient electrochemical OER catalysts. In order to gain an insight into the behavior of $NiCo_2O_4$/CNTs during the oxygen

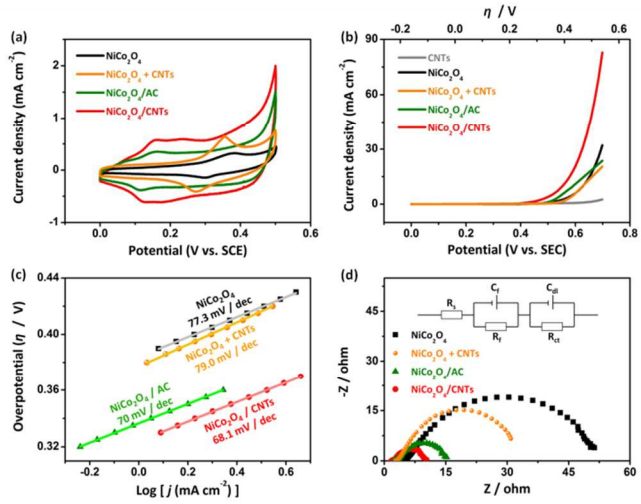

Figure 5. (a) CV curves, (b) Polarization curves, (c) Tafel plots, and (d) Nyquist plots of hierarchical $NiCo_2O_4$/CNTs, $NiCo_2O_4$/AC, the physical mixture of $NiCo_2O_4$ and CNTs and pure $NiCo_2O_4$.

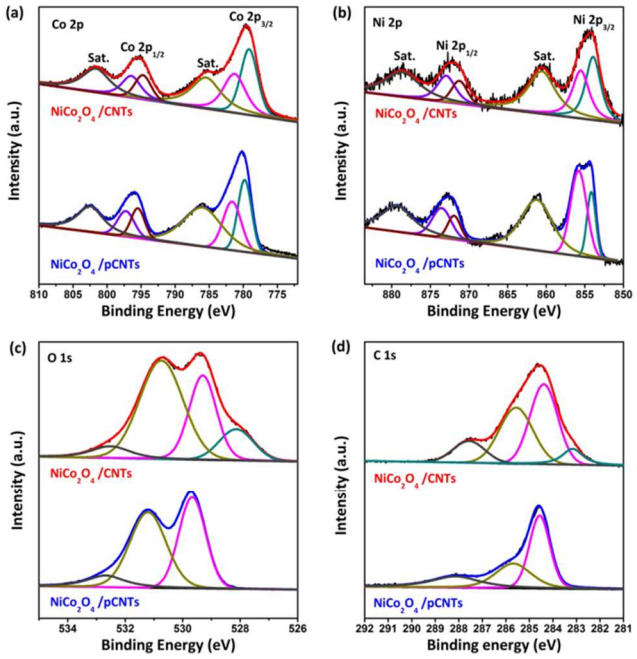

Figure 6. XPS spectra for the hierarchical $NiCo_2O_4$/CNTs and $NiCo_2O_4$/pCNTs.

evolution, Nyquist plots of the EIS spectra carried out at 0.56 V in Figure 5d. The inset shows the equivalent circuit used to obtain charge transfer resistance of the OER catalysts. R_s is the resistance of the electrolyte. R_f is the resistance of the catalysts layer and C_f is the capacitance. C_{dl} is the double layer capacitance and R_{ct} is the charge transfer resistance. In the high frequency region, the resistance is related to the uncompensated solution resistance, which is comparable for all catalysts.[36] The charge transfer resistances (R_{ct}) obtained from the fitted equivalent circuit give an interpretation of the reaction kinetics. The hierarchical $NiCo_2O_4$/CNTs shows much less charge transfer resistance about 6.9 Ω, while $NiCo_2O_4$/AC has an intermediate charge transfer resistance (11.1 Ω), and the pure $NiCo_2O_4$ exhibits the largest resistance of 46.0 Ω. R_{ct} follows the order: $NiCo_2O_4$/CNTs < $NiCo_2O_4$/AC < $NiCo_2O_4$ + CNTs < pure $NiCo_2O_4$. This result may be mainly attributed to the high electrical conductivity of the multi-walled CNTs. To determine the Coulombic efficiency of OER catalyzed by $NiCo_2O_4$/CNTs, the amounts of oxygen produced during electrolysis at 0.01 A was measured for 1 hour (Figure S5). The amount of oxygen produced matches well with the charge consumed assuming 4 electrons for one O_2. This result indicates that $NiCo_2O_4$/CNTs possesses a highly coulombic efficiency for the OER process.

In order to further investigate the function of the oxygen-enriched groups, XPS measurements were performed. As shown in Figure 6, Co 2p emission spectrum of three samples were best fitted with two spin-orbit doublets and two shakeup satellite (identified as "Sat."), where peaks at about 794.75 eV and 779 eV are ascribed to Co^{3+}, whereas peaks at about 796.5 eV and 781 eV are associated with Co^{2+}.[37] Clearly, two kinds of Ni species can be observed that peaks at about 871 eV and 855.5 eV are ascribed to Ni^{3+}, meanwhile peaks at about 873 eV and 854 eV pertain to Ni^{2+}.[38] The spectrum for the O 1s region shows three contributions in all the samples except that $NiCo_2O_4$/CNTs has four contributions. The fitting peak at 529.5 eV is typical of

metal-oxygen bonds.[39] Sitting at 531 eV, the component is usually associated with oxygen in OH^- groups, indicating that the presence of the sample is hydroxylated to some extent as a result of either surface hydroxide or substitution of oxygen atoms at the surface by hydroxyl groups.[40,41] The well-resolved peak around 532.4 eV corresponds to the multiplicity of physic/chemisorbed water at the surface or the bond of C=O, O−C=O.[42] Notably, the peak at 528.1 eV is presented in $NiCo_2O_4$/CNTs, which may correspond to the lattice oxygen in MO_2 (M = Ni or Co), an active intermediate product for OER, caused by the establishment of carboxyl-metal coordination reducing the electron cloud density around the metal. Figure 6d displays the C 1s spectra of $NiCo_2O_4$/CNTs and $NiCo_2O_4$/pCNTs. The previous studies assigned the binding energy of the C−C and C−H bonds to be at 284.5-285 eV, while peaks at 285.5 eV and 288 eV are assigned to the carbon-net defects, attributed to the C atom no longer in the regular tubular structure and different oxygen-containing moieties respectively.[43-44] Obviously, the C 1s peak of $NiCo_2O_4$/CNTs has two remarkable differences compared to $NiCo_2O_4$/pCNTs: the carbon-net defect is broader and a new peak arise around at 283.1 eV may be contributing to C−C bonds in carbide. Table S2 gives the summary of XPS data for $NiCo_2O_4$/CNTs, $NiCo_2O_4$/pCNTs, and the pure $NiCo_2O_4$. It can be clearly observed that $NiCo_2O_4$/CNTs have the largest proportion of Co/Ni. On the other hand, the Co^{3+}/Co^{2+} ratio in these three samples are similar, nevertheless, the Ni^{3+}/Ni^{2+} is quite distinctive that the highest proportion belongs to the pure $NiCo_2O_4$ and the proportion of the other two sample are 2:1 and 1:1, respectively. These results may be mainly attributed to the difference ratio of Co/Ni on the surface layer among these samples, and the cobalt oxide covering the outside surface of $NiCo_2O_4$/CNTs prevents the oxidization of Ni^{2+}.

The proposed mechanism of the surface layer combination is presented in Scheme S1. As presented in Scheme S1 (Ⅰ), when the surface has no any functional group with coordination ability, the hydroxide precipitation caused by the ammonium assemble by the Co/Ni ratio as 2:1 that the composition of the sample are homogeneous. However, after the oxidation, the carboxyl having the coordination ability to Ni and Co alters the proportion of these two species which comes to 1:1. With the precipitation covered, the assembly of Co and Ni conducts according to the rest proportion of Co/Ni, forming another hydroxide layer that the ratio of Co/Ni is inhomogeneous [Scheme S1 (Ⅱ)]. However, once the amount of the functional group decreases on the pristine multi-walled CNTs, the consumption of the coordinated Co and Ni will reduce with little impact to the Co/Ni ratio [Scheme S1 (Ⅲ)].

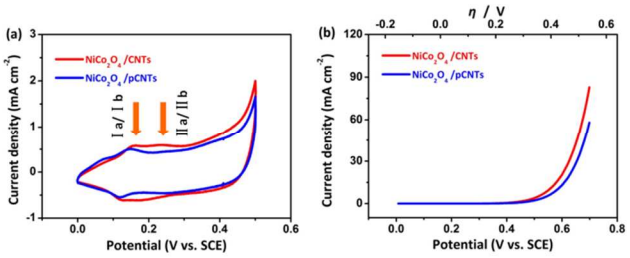

Figure 7. (a) CV curves of $NiCo_2O_4$/CNTs and $NiCo_2O_4$/pCNTs; (b) Polarization curves of $NiCo_2O_4$/CNTs and $NiCo_2O_4$/pCNTs.

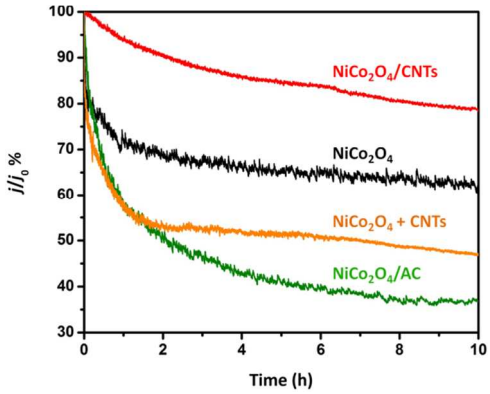

Figure 8. Chronoamperometry data recorded on the hierarchical $NiCo_2O_4$/CNTs, $NiCo_2O_4$/AC, the physical mixture of $NiCo_2O_4$ and CNTs and pure $NiCo_2O_4$ at 0.56 V measured in 1M KOH.

The difference of electrocatalytic performance caused by the surface Co/Ni ratio between $NiCo_2O_4$/CNTs and $NiCo_2O_4$/pCNTs is probed in the OER electrocatalysis. Firstly, we recorded CV curves in saturated 1 M KOH with the scan rate of 5 mV s^{-1} in Figure 7a. Both hybrids show similar redox couple (Ⅰa/Ⅰb), but $NiCo_2O_4$/CNTs has another redox couple (Ⅱa/Ⅱb). The generation of the redox peaks (Ⅱa/Ⅱb) may be attributed to the rise of the metal ion valence state, which was increased by plenty of carboxyl on the multi-walled CNTs that the density of the metal electron cloud decreases. The redox couples can be assigned to:[45]

□a/□b: $MO + OH^- \leftrightarrow MOOH + e^-$

□a/□b: $MOOH + OH^- \leftrightarrow MO_2 + H_2O + e^-$

□a/□b: $2MO_2 \rightarrow 2MO + O_2$

Secondly, the OER pathways catalyzed by $NiCo_2O_4$/CNTs and $NiCo_2O_4$/pCNTs were also investigated in Figure 7b. $NiCo_2O_4$/CNTs exhibits significantly higher OER current density than $NiCo_2O_4$/pCNTs. As the previous reported literature, the surface of Co undergoes progressive oxidation with the formation of Co^{4+} species, at which oxygen evolution occurs. Thus, with the existence of the oxygen-enriched groups on the CNTs increasing some essential intermediates, the abundance of cobalt oxide and the MO_2 existing on the surface of $NiCo_2O_4$/CNTs open more active site for OER process and improve electrocatalytic activity.[46]

High stability toward OER is of great significance for the energy conversion and storage systems, and the chronoamperometric technique is an effective means to examine the electrochemical stability of electrocatalyst. The long-term electrochemical stability of $NiCo_2O_4$/CNTs, $NiCo_2O_4$/AC, $NiCo_2O_4$ + CNTs and pure $NiCo_2O_4$ electrodes towards water splitting were investigated in 1 M KOH solution at 0.56 V for 10 h. As presented in Figure 6, $NiCo_2O_4$/CNTs exhibits a slight anodic current attenuation of 8% within 1 h, whereas $NiCo_2O_4$/AC and pure $NiCo_2O_4$ display a larger current attenuation of 40% and 27%, respectively. After 10 h, $NiCo_2O_4$/CNTs remained a higher current density (83%), revealing the high stability of $NiCo_2O_4$/CNTs. The SEM images of $NiCo_2O_4$/CNTs, $NiCo_2O_4$/AC and $NiCo_2O_4$ after the stability measurement were shown in the Supporting Information (Figure

S7, Figure S8, Figure S9). As can be seen, after the stability measurement the morphology of $NiCo_2O_4$/CNTs changed slightly. However, the morphology of $NiCo_2O_4$/AC and $NiCo_2O_4$ change is obvious. These results indicate the poor stability for $NiCo_2O_4$/AC and $NiCo_2O_4$. In addition, the XPS spectra for $NiCo_2O_4$/CNTs have also been tested (Figure S10). From the XPS spectra, $NiCo_2O_4$/CNTs still possessed the high ratio of Co/Ni (about 2.7) after the stability measurement. Moreover, the valence state ratio of Ni is 0.31 for Ni^{3+}/Ni^{2+}, and that of Co is 1.05 for Co^{3+}/Co^{2+}. Compared with the corresponding XPS results which were tested before the stability measurement, the slightly change of the valence state and the ratio of Co/Ni in the surface further confirm the high stability of $NiCo_2O_4$/CNTs

Conclusion

In summary, the hierarchical $NiCo_2O_4$/CNTs hybrid has been synthesized by one-pot synthesis method. The selective nucleation of $NiCo_2O_4$ on CNTs was well controlled by readily adjusting the pH of solution. The as-prepared hierarchical $NiCo_2O_4$/CNTs exhibits superior OER activity and high stability, which may be mainly attributed to the remarkable conductivity, large specific surface area of CNTs and the synergistic effect between the oxygen-enriched group and metal ions. This work offers a novel molecular-scale hybridizing strategy to develop robust and low-cost catalysts with high catalytic efficiency and high durability for potential energy conversion and storage applications.

Acknowledgements

The authors acknowledge the financial support of this work by Natural Science Foundations of China (Grant No. 21306030), the Natural Science Foundations of Guangdong Province (Grant No. s2013040015229 and 2014A030313520), Program Foundation of the second batch of innovation teams of Guangzhou Bureau of Education (Grant No. 13C04), Scientific Research Project of Guangzhou Municipal Colleges and Universities (Grant No. 1201410618), and the Fresh Talent Program of Guangzhou University (Grant No. 201302).

Notes and references

School of Chemistry and Chemical Engineering/Guangzhou Key Laboratory for Environmentally Functional Materials and Technology, Guangzhou University, Guangzhou Higher Education Mega Center, Waihuan Xi Road No. 230, China 510006
Fax: 86-20-39366908; Tel: 86-20-39366908;
E-mail:lzqgzu@gzhu.edu.cn (Z.-Q. Liu)

[1] T. W. Kim and K. S. Choi, *Science*, 2014, **343**, 990-994.
[2] M. Zhang, M. Respinis and H. Frei, *Nat. Mater.*, 2014, **6**, 362-367.
[3] F. Jiao and H. Frei, *Angew. Chem. Int. Ed.*, 2009, **48**, 1841-1844.
[4] B. S. Yeo and A. T. Bell, *J. Am. Chem. Soc.*, 2011, **133**, 5587-5593.
[5] M. G. Walter, E. L. Warren, J. R. McKone, S. W. Boettcher, Q. Mi, E. A. Santori and N. S. Lewis, *Chem. Rev.*, 2010, **110**, 6446-6473.
[6] F. Y. Cheng and J. Chen, *Chem. Soc. Rev.*, 2012, **41**, 2172-2192.
[7] H. L. Wang and H. J. Dai, *Chem. Soc. Rev.*, 2013, **42**, 3088-3113.
[8] Y. M. Lee, J. Suntivich, K. J. May, E. E. Perry and H. Y. Shao, *J. Phys. Chem. Lett.*, 2012, **3**, 399-404.
[9] Y. Liang, H. Wang, J. Zhou, Y. Li, J. Wang, T. Regier and H. Dai, *J. Am. Chem. Soc.*, 2012, **134**, 3517-3523.
[10] X. Wu and K. Scott, *J. Power Sources*, 2012, **206**, 14-19.
[11] T. Y. Ma, S. Dai, M. Jaroniec and S. Z. Qiao, *J. Am. Chem. Soc.*, 2014, **136**, 13925-13931.
[12] C. Xiao, X. Lu and C. Zhao, *Chem. Commun.*, 2014, **50**, 10122-10125.
[13] T. W. Kim, M. A. Woo, M. Regis and K. S. Choi, *J. Phys. Chem. Lett.*, 2014, **5**, 2370-2374.
[14] X. Wu and K. Scott, *J. Mater. Chem.*, 2011, **21**, 12344-12351.
[15] H. Shi and G. Zhao, *J. Phys. Chem. C*, 2014, **118**, 25939-25946.
[16] L. X. Zhang, S. L. Zhang, K. J. Zhang, G. J. Xu, X. He, S. M. Dong, Z. H. Liu, C. S. Huang, L. Gu and G. L. Cui, *Chem. Commun.*, 2013, **49**, 3540-3542.
[17] J. F. Li, S. L. Xiong, Y. R. Liu, Z. C. Ju and Y. T. Qian, *ACS Appl. Mater. Interfaces*, 2013, **5**, 981-988.
[18] Z. Q. Liu, Q. Z. Xu, J. Y. Wang, N. Li, S. H. Guo, Y. Z. Su, H. J. Wang, J. H. Zhang and S. Chen, *Int. J. Hydrogen Energy*, 2013, **38,** 6657-6662.
[19] G. Q. Zhang, B. Y. Xia, X. Wang and X. W. Lou, *Adv. Mater.*, 2014, **26**, 2408-2412.
[20] M. Cabo, E. Pellicer, E. Rossinyol, M. Estrader, A. Lopez. Ortega, J. Nogues, O. Castell, S. Surinach and M. D. Baro, *J. Mater. Chem.*, 2010, **20**, 7021-7028.
[21] Z. Q. Liu, K. Xiao, N. Li, Y. Z. Su, H. J. Wang and S. Chen, *RSC Adv.*, 2013, **3**, 4372-4380.
[22] G. Q. Zhang and X. W. Lou, *Adv. Mater.*, 2013, **25**, 976-979.
[23] Y. G. Li, P. Hasin and Y. Y. Wu, *Adv. Mater.*, 2010, **22**, 1926-1929.
[24] D. U. Lee, B. J. Kim and Z. W. Chen, *J. Mater. Chem. A*, 2013, **1**, 4754-4762.
[25] J. Chao, F. L. Lu, X. C. Cao, Z. R. Yang and R. Z. Yang, *J. Mater. Chem. A*, 2013, **1**, 12170-12177.
[26] Y. Z. Su, Q. Z. Xu, G. F. Chen, H. Cheng, N. Li, Z. Q. Liu, *Electrochim. Acta*, 2015, DOI: 10.1016/j.electacta.2015.06.092.
[27] S. Chen and S. Z. Qiao, *ACS Nano*, 2013, **7**, 10190-10196.
[28] I. Dumitrescu, P. R. Unwin and J. V. Macpherson, *Chem. Commun.*, 2009, **45**, 6886-6901.
[29] J. M. Schnorr and T. M. Swager, *Chem. Mater.*, 2011, **23**, 646-657.
[30] X. Chen, H. Zhu, Y. C. Chen, Y. Shang, A. Cao, L. Hu and G. W. Rublo, *ACS Nano*, 2012, **6**, 7948-7955.
[31] Y. Cheng, C. Liu, H. M. Cheng and S. P. Jiang, *ACS Appl. Mater. Interfaces*, 2014, **6**, 10089-10098.
[32] J. Wei, Y. Liu, Y. Ding, C. Luo, X. Du and J. Lin, *Chem. Commun.*, 2014, **50**, 11938-11941.
[33] X. M. Ge, Y. Y. Liu, F. W. Thomas Goh, T. S. Andy Hor, Y. Zong, P. Xiao, Z. Zhang, S. H. Lim, B. Li, X. Wang and Z. L. Liu, *ACS Appl. Mater. Interfaces*, 2014, **6**, 12684-12691.
[34] Y. Y. Liang, Y. G. Li, H. L. Wang and H. J. Dai, *J. Am. Chem. Soc.*, 2013, **135**, 2013-2036.
[35] H. Zhang, H. Qiao, H. Y. Wang, N. Zhou, J. J. Chen, Y. G. Tang, J. S. Li and C. H. Huang, *Nanoscale*, 2014, **6**, 10235-10242.
[36] Y. T. Meng, W. Q. Song, H. Huang, Z. Ren, S. Y. Chen and L. S. Steven, *J. Am. Chem. Soc.*, 2014, **136**, 11452-11464.
[37] B. Cui, H. Lin, Y. Z. Liu, J. B. Li, P. Sun, X. C. Zhao and C. J. Liu, *J. Phys. Chem. C*, 2009, **113**, 14083-14087.
[38] C. Yuan, J. Li, L. Hou, X. Zhang, L. Shen and X. W. Lou, *Adv. Funct. Mater.*, 2012, **22**, 4592-4597.
[39] C. Yuan, J. Li, L. Hou, L. Yang, L. Shen and X. Zhang, *J. Mater. Chem.*, 2012, **22**, 16084-16090.
[40] Y. E. Roginskaya, O. V. Morozova, E. N. Lubnin, Y. E. Ulitina, G. V. Lopukhova and S. Trasatti, *Langmuir*, 1997, **13**, 4621-4627.
[41] V. M. Jimenez, A. Fernandez, J. P. Espinos and A. R. Gonzalez-Elipe, *J. Electron Spectrosc. Relat. Phenom.*, 1995, **71**, 61-71.
[42] V. Datsyuk, M. Kalyva, K. Papagelis, J. Parthenios, D. Tasis, A. Siokou, I. Kallitsis and C. Galiotis, *Carbon*, 2008, **46**, 833-840.
[43] N. Zhang, J. Xie and V. K. Varadan, *Smart Mater. Struct.*, 2002, **11**, 962-965.
[44] G. Beamson, A. Bunn and D. Briggs, *Surf. Interface Anal.*, 1991, **17**, 105-115.
[45] C. Bocca, A. Barbucci, M. Delucchi and G. Cerisola, *Int. J. Hydrogen Energy*, 1999, **24**, 21-26.
[46] X. J. Liu, J. F. Liu, Y. P. Li, Y. J. Li and X. M. Sun, *ChemCatChem*, 2014, **6**, 2501-2506.

GRAPHICAL ABSTRACT